LICENTIATE THESIS

Towards Discrete Element Modelling of Rock Drilling

Albin Wessling

Solid Mechanics

LULEÅ UNIVERSITY OF TECHNOLOGY

Towards Discrete Element Modelling of Rock Drilling

Albin Wessling

Division of Solid Mechanics
Department of Engineering Sciences and Mathematics
Luleå University of Technology
Luleå, Sweden

Licentiate Thesis in Solid Mechanics

Preface

The work within this thesis has been carried out at the Division of Solid Mechanics, Department of Engineering Sciences and Mathematics at Luleå University of Technology, Sweden. The Horizon 2020 project GEOFIT is acknowledged for financing the work within this thesis, grant agreement number 792210.

There are many people that contributed to the completion of this thesis. Foremost, I would like to express my gratitude to my supervisors, Assoc. Prof. Jörgen Kajberg, Prof. Pär Jonsén and Dr. Simon Larsson, for entrusting me with this opportunity and subsequently guiding and supporting me throughout my first few years at the division. I also want to thank Jan Granström and Ulf Stenman for the help with the experiments. Furthermore, I am very grateful that I got to work with my inspiring colleagues at the Solid Mechanics division. Finally, this work would not have been possible without the support from my family and friends back in Gävleborg and Stockholm.

Luleå, May 2021

Abstract

The method of percussive rotary drilling is recognized as the most efficient method for hard rock drilling. Despite the clear advantages over conventional rotary methods, there are still uncertainties associated with percussive rotary drilling. For geothermal applications, it is estimated that 50 % of the total cost per installed megawatt of energy is associated with drilling and well construction, with drill bit wear being a predominant cost factor. Numerical modelling and simulation of rock drilling, calibrated and validated towards rigorous experiments, can give insight into the rock drilling process. This thesis is focused on the prerequisites of numerical simulations of rock drilling, i.e. the development of a numerical model and experimental characterization of rock materials. A new approach for modelling brittle heterogeneous materials was developed in this work. The model is based on the Bonded Particle Method (BPM) for the Discrete Element Method (DEM), where heterogeneity is introduced in two ways. Firstly, the material grains are represented by random, irregular ellipsoids that are distributed throughout the body. Secondly, these grains are constructed using the BPM-DEM approach with micromechanical parameters governed by the Weibull distribution. The model was applied to the Brazilian Disc Test (BDT), where crack initiation, propagation, coalescence and branching could be investigated for different levels of heterogeneity and intergranular cement strengths. The initiation and propagation of the cracks were found to be highly dependent on the level of heterogeneity and cement strengths. In the experimental study, the static and dynamic properties of two rock materials - Kuru grey granite and Kuru black diorite - were obtained from uniaxial compression and indirect tension tests. A Split-Hopkinson Pressure Bar was used to obtain the dynamic properties. Using high-speed photography with frame rate 663,000 fps, the crack initiation and propagation could be studied in detail, and the full-field exterior deformation fields of the samples were evaluated by using digital image correlation. From the high-speed images, the onset of unstable crack growth was detected. The crack-damage stresses, associated with unstable crack growth, was approx. 90 % of the peak strength in the dynamic compression tests, whereas the tensile crack-damage stress was approx 70 % of the tensile peak strength.

Thesis

This is a compilation thesis consisting of a synopsis and the following scientific articles:

Paper A:
Albin Wessling, Simon Larsson, Pär Jonsén, Jörgen Kajberg. A statistical DEM approach for modelling heterogeneous brittle materials. *Submitted to Computational Particle Mechanics, Springer*

Paper B:
Albin Wessling, Jörgen Kajberg. Static and Dynamic Properties of Kuru Black Diorite and Grey Granite Using Full-Field Deformation Measurements. *To be submitted*

Contributions by the present author

The thesis author was responsible for the main part of the work regarding experiments and modelling with support from the co-authors.

Contents

Synopsis **1**

Chapter 1 – Introduction 3
1.1 Background and motivation . . . 3
1.2 Scientific background . . . 4
1.3 Objective and scope . . . 6

Chapter 2 – Rock materials 7

Chapter 3 – Experimental methods 9
3.1 Failure of rocks . . . 9
3.2 Static uniaxial compression test . . . 10
3.3 Static Brazilian Disc Test . . . 11
3.4 Split-Hopkinson Pressure Bar . . . 12
3.5 Digital image correlation . . . 14

Chapter 4 – Modelling 15
4.1 The Bonded Discrete Element Method . . . 15
4.2 A new approach for modelling rock . . . 17

Chapter 5 – Summary of appended papers 21
5.1 Paper A: A Statistical DEM Approach for Modelling Heterogeneous Brittle Materials . . . 21
5.2 Paper B: Static and Dynamic Properties of Diorite and Granite . . . 22

Chapter 6 – Discussion, conclusions and outlook 25

References 27

Appended Papers **33**

Paper A 35

Paper B 55

Synopsis

Chapter 1

Introduction

The purpose of this first chapter of the thesis is to introduce the reader to the content of the appended papers. This includes background and motivation, the scientific background, objective and scope and limitations. The general context, of which the thesis aims to contribute to, is also described.

1.1 Background and motivation

Percussive drilling can be traced back 2000 years to the Sichuan province, China, where it was used for drilling salt wells. By using man powered percussive drilling rigs made from iron and bamboo pipes, the salt miners were able to reach an impressive depth of 140 m. For these larger wells, it could take two to three generations of workers to complete the work. Even today, farmers in rural China use this ancient drilling method for drilling water wells [1]. In the 19th and 20th century, steam powered and pneumatic drilling tools were invented, which revolutionized the industry [2].

Today, percussive rotary drilling (PRD) is still recognized as the most efficient for hard rock excavation, surpassing conventional rotary methods. The most common version of PRD is the down-the-hole (DTH) method, where the drill bit is typically made from high-strength low-alloy steel with cemented carbide inserts situated at the face of the bit. A piston strikes the tail of the drill bit, generating a compressive stress wave that propagates through the bit body and pushes the button inserts into the rock surface. Initially, microcracks are formed and a crushed zone of small particles is created directly underneath the contact point. When the button inserts penetrate the rock further, major cracks begin to develop. For spherical intenders, these cracks are initiated just outside the contact area. The crack growth is, however, still restricted. As the inserts penetrate even

deeper and the critical energy level for full crack propagation is reached, rapid and spontaneous crack propagation occurs. When the crack tip reaches a depth where the tensile driving force is not large enough to allow for propagation, the crack becomes stable and is said to be well developed. As the force generated from the indentation reaches a sufficient level, rock cuttings are created by lateral cracks propagating from the indenter tips to the rock surface, typically forming an angle between 120° and 150° [3]. These rock cuttings are then flushed from the hole, typically using compressed air or water. The drill bit is then rotated and the process is repeated at a new rock surface. It is well understood that this initiation, propagation and coalescence of cracks are the governing factors for the rock excavation process [4–7].

It has been shown that PRD is between 2.3 to 7.3 times faster than rotary drilling when drilling in medium-hard rock [8]. Other advantages of the PRD method includes lower weight-on-bit and decreased abrasive wear due to less contact time with the rock. Despite the clear advantages, there are still some uncertainties with this method. For example, by increasing the impact energy of the drill bit an increase in ROP may be obtained but the potential increase in wear rate of the drill bit may not be economically motivated. For geothermal applications, the wear of the drill bits has always been a dominant cost factor, not only due to the direct material and personnel costs associated with a broken down bit, but also due to the loss off drilling efficiency as the drill bit has been worn out [9]. This loss in efficiency due to wear is especially true for the cemented carbide inserts that play a central role in the initation of cracks. Thus, there is a trade-off between ROP and wear rate. Further, the optimal drilling parameters change with drilling depth since the confining pressure and subsequently rock strength increases [10]. These optimal drilling parameters often rely on the field experience of the operator and is seldom based on scientific theory or numerical simulations. By evaluating the process of rock fracture, both experimentally and numerically, insights about rock drilling can be gained. These insights can in turn aid in obtaining these optimal drilling parameters.

1.2 Scientific background

The thesis is focused on experimental and numerical studies of the rock fracture process. This topic is of vital importance for several rock excavation applications, such as drilling in mining and geothermal applications. The rock fracture process has been studied for a long time, and with recent experimental and numerical advances, it is still an active area of research today.

The perhaps oldest method for experimental characterization of rock is the Uniaxial Compression Test (UCT) [11], which has been widely used to study rock

materials in quasi-static conditions [12–14]. For tensile testing of rock materials, the Brazilian Disc Test (BDT) is most commonly used [15, 16]. Although only being an indirect measurement of the tensile strength, the BDT is preferred over direct methods due to its simplicity [17] and its validity and applicability have been studied extensively [18–21]. More recently, the BDT has been used for estimation of the tensile elastic modulus [22], tensile Poisson's ratio [23] and confined tensile strength [24] of rock materials.

The fracture process of rock materials has been found to be significantly different at dynamic loading. Once the required stress for crack initiation is reached in a static test, the weakest crack starts growing and the stored elastic energy continues to rapidly drive the crack forward. For dynamic loading, however, the inertia associated with crack tip opening limits the propagation, and as the load is rapidly increasing, new cracks are initiated before previous cracks are unstable [25]. In this way, the dynamic fracture process of rock is characterized by multiple cracks initiating almost simultaneously. The Split-Hopkinson Pressure Bar (SHPB) [26] is commonly used to study the dynamic behaviour of rock materials, and has been used to study uniaxial compression [27], confined compression [10, 28], indirect tension [29] and other rock related experiments [30]. The use of High-Speed Photography (HSP) in combination with the SHPB dates back to Perkins and Green [31] in 1968 and can complement the strain gauge data with information about fracture initiation and propagation. More recently, HSP has been used to evaluate the crack initiation and propagation in the dynamic BDT [32–35]. Furthermore, by combining HSP with Digital Image Correlation [36, 37], the exterior full-field measurements of sample deformation can be obtained. The HSP-DIC approach has been used to evaluate the crack propagation speed in red sandstone [38] and the UCT, BDT and Notched Semi-Circular Bend (NSCB) of marble [39].

With regards to numerical modelling of rock fracture, the methods can be divided into two groups - direct and indirect methods - depending on how damage is represented. The traditional Finite Element Method (FEM) is an indirect method, where the material is idealized as a continuum and various constitutive and damage models are employed in order to model the fracture process. As an example, [40] investigated the fracture of granite with FEM with a damage model in tension, a plasticity model in compression and a weakest link approach based on Weibull [41] to distribute defects in the model. This model has later been used to study the tensile response of granite subjected to high strain rates [42].

In contrast to the indirect approaches, direct approaches represents damage directly by tracking the formation and propagation of each microcrack. The Bonded-Particle Model (BPM) [43] for the Discrete Element Method [44] is an example of a direct method. Here, the damage is represented by the breakage of linear-elastic bonds between rigid spheres that constitute the rock material. Cracks initiate

spontaneously on a micromechanical scale through the breakage of these bonds, and propagate in the media through more broken bonds and coalesce with other cracks to form macroscopic fracture planes. In this way, the BPM is able to naturally describe the initiation, propagation, branching and coalescence of cracks in rock materials. The BPM has been applied to a wide range of industrial problems involving brittle fracture, such as rock indentation [45, 46] and rock cutting [47, 48]. A challenge with the original formulation of BPM is the low amount of grain interlocking from spherical grains, resulting in unrealistically low compression to tension strength ratios, making it impossible to match both the compressive and tensile strength for some cases. Previous authors have suggested solutions to this problem, such as utilizing clumped particles [49], increasing the interlocking range [50], using a displacement-softening contact law [51] and employing smooth-joint interfaces that allow sliding along specified joint directions [52]. Also, the BPM has later been extended to the Grain-Based Model [53] that incorporates polygonal elements and smooth-joint interfaces.

1.3 Objective and scope

The objective of this thesis is to contribute to the knowledge of the rock fracture process, using both numerical and experimental methods. To this end, two research questions can be formulated: "How can particle-based methods increase our knowledge about the rock fracturing processes?" and "How can experimental techniques be used to characterize rock at conditions found in rock drilling?". The work can be viewed as the prerequisites of a numerical simulation of rock drilling. Therefore, the scope of this thesis work is to develop the numerical approach for describing the heterogeneous nature of rock as well as experimentally characterising rock materials subjected to high loading rates. The experimental work is limited to two types of rock materials, Kuru grey granite and Kuru black diorite, that are commonly encountered during geothermal rock drilling. The numerical model developed within this thesis was not calibrated or validated towards a specific rock material. Instead, the focus was to demonstrate the capability for brittle and heterogeneous materials in general.

Chapter 2

Rock materials

The wear of rock drilling bits is highly dependent on the target material - rock. The word **rock** is a wide term that may refer to everything from single minerals to compositions of several minerals with a wide range of grain sizes (μm to dm) The rock can be divided into three main groups depending on its origins; *Igneous*, *sedimentary* and *metamorphic* rocks [3, 54, 55]. Igneous rocks are formed by the solidification of magma from the earth crust. Depending on where the solidification takes place, the igneous rock is either *intrusive* or *extrusive*. Intrusive rocks are formed when the magma is solidified slowly underneath the earth surface, typically resulting in rock with coarse mineral grains visible to the naked eye. On the other hand, extrusive igneous rocks are formed when the magma is cooled quickly at the earth surface, which produces fine-grained rock with very small crystals (if any at all). Granite and diorite are examples of intrusive igneous rocks, while basalt is an example of extrusive igneous rock. Sedimentary rocks are formed from the accumulated deposition of minerals. These minerals have been transported, e.g. via wind, ice, water and glaciers, from a source area. The different sediments are transformed into rock via the process of cementing, typically by calcite or silica, of the different fragments followed by lithification. The sedimentary rocks are formed in layers known as *strata* or *layers*. Depending on the sediment source, the grain size varies from very fine to very coarse. As a rock type is subjected to heat and pressure, a severe change in chemical composition and structure may occur, giving rise to metamorphic rock. The original rock type may be igneous, sedimentary or metamorphic. For example, quartzite is formed by the metamorphic transformation of sandstone, or marble that is formed by the metamorphic transformation of limestone.

In geothermal applications, borehole depths of several hundred metres are common [57], and with connection to what was stated above, a wide range of rock materials may be encountered during the drilling process. With regards to the

Table 2.1: Mohs scale of hardness for some minerals [56].

Mohs hardness	Mineral
1	Talc
2	Gypsum
3	Calcite
4	Fluorite
5	Apatite
6	Orthoclase Feldspar
7	Quartz
8	Topaz
9	Corundum
10	Diamond

Table 2.2: Mineral composition of Kuru Grey Granite (KGG).

Mineral	Plagioclase	Quartz	Potassium feldspar	Biotite	Muscovite	Other
wt %	32.6	31.0	30.8	3.5	1.2	0.9

wear of drilling bits, the problematic rock materials are those with hard constituent minerals. A common measurement of hardness for minerals is Mohs scale, as created by Friedrich Mohs in 1812. The minerals are ranked in a qualitative manner, according to which mineral is able to scratch which other mineral, see Table 2.1. Although diamond and corundum are ranked the highest, the mineral most frequently associated with wear in drilling bits is quartz [3, 9, 54]. Kuru grey granite (KGG), which is one of the rocks subject to experimental characterization in this thesis, contains 31 % quartz and 32.6 % plagioclase, which is a mineral within the feldspar group, see Table 2.2. The other rock material investigated in this thesis, Kuru black diorite, does not contain any quartz, but contains 57 % plagioclase, see Table 2.3. Thus, both of the investigated rock materials are problematic with regards to the rock drilling process.

Table 2.3: Mineral composition of Kuru Black Diorite (KBD).

Mineral	Plagioclase	Biotite	Amphibians	Ilmenite	Climopyroxen	Other
wt %	57.0	21.0	10.0	6.4	6.0	4.0

Chapter 3

Experimental methods

Due to the dynamic nature of rock drilling, the loading rate dependencies of the rock materials have to be determined. For this, two experiments - Uniaxial Compression Test (BDT) and Brazilian Disc Test (BDT) - are employed. Further, the initation, propagation and coalescence of cracks also need to be investigated. It is important to note, however, that besides the direct mechanical response, discontinuities are present in the rock which greatly affects the behaviour. On a microscopic scale, these discontinuities are made up of microcracks, pores and the grain boundaries cementing the different mineral grains together. Further, the grains can exhibit geometrical heterogeneities due to grain size, shape and distribution, but also mechanical heterogeneity due to different strengths and elastic properties. On a much larger scale, up to a few hundred meters, joints, faults, bedding planes and large cracks are examples of discontinuities. Aside from affecting the strength, these discontinuities will of course also introduces anisotropic behaviour in the rock mass [11]. This chapter covers the experimental procedures used to characterize the rock, both in static and dynamic loading.

3.1 Failure of rocks

By considering a stress vs strain curve from a UCT, Brace et al. [58] among others have shown that the response can be divided into five regions according to Figure 3.1. The initial region represents closure of any existing microcracks. The second region is considered to be homogeneous and elastic. At approx. 50 % of the peak strength, the third region is entered and dilation initiates causing axial cracks, i.e. cracks parallel to the loading direction. This stress level is usually referred to as the crack-initiation stress. In the third region stable crack growth is present. Generally, the cracking turns unstable at a stress level between 70

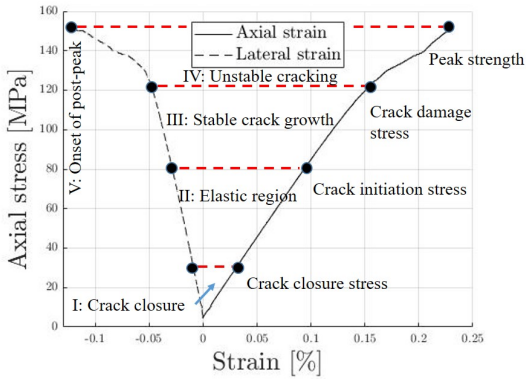

Figure 3.1: Stress vs strain diagram for a Uniaxial Compression Test (UCT) and definition of five stages of deformation, damage and failure.

to 85 % of the peak strength. This level of stress, so-called crack-damage stress, marks the onset of the last stage (region IV) before the final failure and onset of post-peak behaviour (region IV). The crack-damage stress and the peak strength will be determined by the experimental set-ups desribed in the following sections.

3.2 Static uniaxial compression test

Testing of a rock materials resistance to compression is the oldest and most straightforward test for rock [11]. The most common version is the uniaxial compression test where a cylinder is compressed axially until failure. A schematic view of this experiment can be seen in Figure 3.2a. The cylinder is loaded along the axial direction until failure, and the compressive strength is defined as the maximum stress obtained during the test [59]

$$\sigma_c = \frac{F}{A_0} \tag{3.1}$$

where F is the applied load and A_0 is the initial cross-sectional area of the sample. Furthermore, if strain gauges are mounted along the vertical and lateral, see Figure 3.2a, directions, the compressive elastic modulus and Poission's ratio can be measured as well. The sample may fail due to axial splitting, multiple fracturing or shearing along one or several planes. For metamorphic rocks, the preferred failure mode has been reported to be along the foliations, while for granite, multiple fracturing and axial splitting were reported to be most common [13].

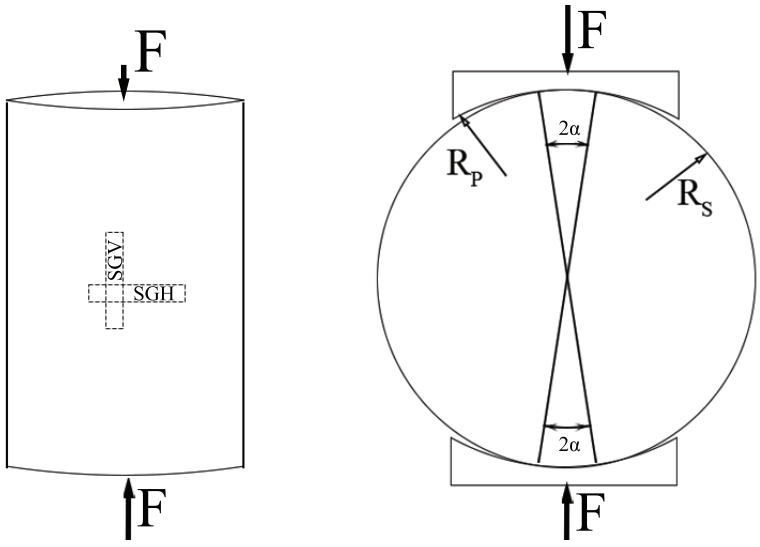

(a) (b)

Figure 3.2: The uniaxial compression test (a) and Brazilian disc test (b).

3.3 Static Brazilian Disc Test

The diametral compression test, or Brazilian Disc Test (BDT), is an experimental method for measuring the indirect tensile strength of brittle materials such as rocks and concretes and was formulated independently by Carneiro [15] and Akazawa [16] in 1943. In the BDT, a circular disc is compressed diametrically over an arc of length 2α, see Figure 3.2b, inducing an indirect tensile stress field in a region around the centre part of the disc. The induced tensile stress close to the center is given by [60, 61]

$$\sigma_{\mathrm{t}} = \frac{2F}{\pi D t} = 0.636\frac{P}{Dt} \tag{3.2}$$

where F is the load distributed over a finite arc of the disc with diameter D and thickness t. In order for the BDT to give a tensile measurement that equals what is measured from direct methods, the main crack splitting the sample has to initiate at the exact disc centre. However, this is seldom the case, as the crack is known to deviate from the centre and even initiating from the loading contact [62, 63]. Therefore, it is important to note that the BDT is an estimation of the tensile strength. However, due to its simplicity, it is still the preferred approach for measuring the tensile strength of rock materials [17]. In order to reduce the

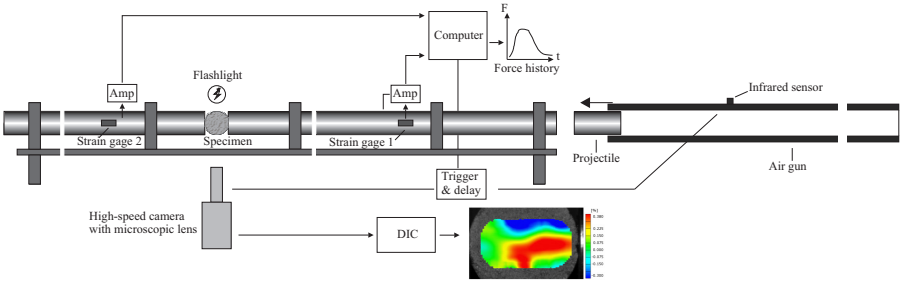

Figure 3.3: The SHPB configuration used for the dynamic testing. Here the set-up is shown for BDT.

stress concentrations at the loading contact, and by extension the amount of cracks initiating from there, curved loading jaws and a cushioning material is often used. For rock materials, it is well known that the elastic modulus and Poission's ratio is different when loading in compression and tension [23]. By measuring the indirect tensile strain at the centre of the BDT and utilizing elastic relationships, [22] demonstrated that the tensile elastic modulus E_t can be obtained as

$$E_{\mathrm{t}} = E_{\mathrm{s}} A^* \tag{3.3}$$

where E_s is the modulus as measured from the indirect tensile stress versus indirect tensile strain curve and A^* is the correction factor given by

$$A^* = \left\{ \left(1 - \frac{D}{L} \arctan \frac{2L}{D} \right) (1 - v) + \frac{2D^2(1+v)}{4L^2 D^2} \right\} \tag{3.4}$$

where D is the disc diameter, ν_c is the compressive Poission's ratio and L is the half length of the strain gauge. With the compressive elastic modulus E_c and Poission's ratio ν_c obtained from the UCT, and the tensile elastic modulus obtained from Eq. 3.3, the tensile Poission's ratio can be given as [23]

$$\nu_t = E_t \frac{\nu_c}{E_c} \tag{3.5}$$

3.4 Split-Hopkinson Pressure Bar

The Split-Hopkinson Pressure Bar (SHPB), or Kolsky bar [26], has over the years been applied to dynamic characterization of various materials at high strain rates ($10^1 - 10^4\ s^{-1}$). Extensive reviews of the SHPB for a wide range of testing of brittle materials can be found in [25, 30]. Within this thesis, the SHPB was used

for the dynamic uniaxial compression and indirect tensile tests.

The SHPB in the Solid Mechanics Laboratory at Luleå University of Technology consists of a 3 m long incident bar and a 2 m long transmitted bar, and the sample is sandwiched between these bars, see Figure 3.3. The bars are made from maraging steel with diameters 25 mm. Thus, the length-to-diameter ratio is 80 and one-dimensional wave theory applies [64]. A cylindrical projectile of length 150 mm and the same material as the bars is accelerated by an air gun and impacts the incident bar, generating a compressive wave that propagates through the incident bar and is partly reflected and transmitted through the sample. The strain histories $\varepsilon_i(t)$, $\varepsilon_r(t)$ and $\varepsilon_t(t)$ of the incident, reflected and transmitted waves are recorded by strain gauges mounted on both bars. In order to capture the initiation and propagation of cracks, a high speed camera, Phantom vision v2512 with a microscopic lens, was used to record the tests.

From one-dimensional wave theory and the definition of one-dimensional strain, the forces at the bar-sample interface are expressed as [64]

$$P_i = AE\left(\varepsilon_i(t) + \varepsilon_r(t)\right) \tag{3.6}$$

and

$$P_t = AE\varepsilon_t(t) \tag{3.7}$$

where P_i and P_t are the forces in the incident and transmitted bar, respectively. A and E are the cross-sectional area and elastic modulus of the bars, respectively. If equilibrium can be assumed, the stress in the UCT can be obtained as

$$\sigma(t) = \frac{AE\varepsilon_t(t)}{A_s} \tag{3.8}$$

where A_s is the cross-sectional area of the sample. The strain rate in the UCT is obtained from

$$\dot{\varepsilon} = \frac{2c_b\varepsilon_r(t)}{l_s} \tag{3.9}$$

where c_b is the longitudinal wave velocity in the bars and l is the length of the UCT sample. Please note the strain convention used here, i.e. a compressive strain is positive. From numerical integration of Eq. 3.9, the strain in the UCT sample is obtained as

$$\varepsilon = \int_{t_{start}}^{t_{end}} \dot{\varepsilon}\, dt \tag{3.10}$$

For the dynamic BDT, the strain rate and strain cannot be obtained through wave theory. Instead, Digital Image Correlation (DIC) was used for measuring the strain, see section 3.5. The indirect tensile stress at the center of the disc, however, can be obtained from Eq. 3.2 if dynamic force equilibrium is assumed.

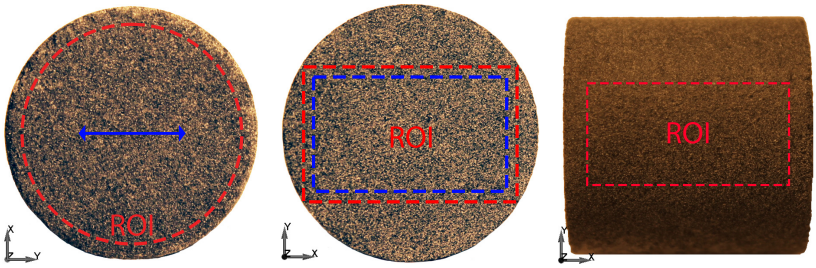

(a) Quasi-Static BDT. (b) Dynamic BDT. (c) Dynamic UCT.

Figure 3.4: Examples of applied speckle pattern for the three samples a-c). Region of interest surrounded by red dashed circle or rectangle. Virtual strain gauge - blue line a). Area for averaging of strain measures blue dashed rectangle b)

3.5 Digital image correlation

Digital Image Correlation (DIC) is a non-contact optical method for full-field exterior measurements of deformations. A key aspect of the DIC is the unique and random black and white pattern on the sample surface that is used to track the displacement of subimages, or facets, between two frames. This random speckle pattern can be obtained by applying a thin layer of black spray paint followed by a thin layer of white spray paint. For more detailed description and applications of the DIC method, see [36, 37].

Within this thesis, the DIC was applied to three experiments - the static and dynamic BDT as well as the dynamic UCT - and the corresponding Region of Interest (ROI) for each experiment is shown in Figure 3.4.

Chapter 4

Modelling

With increased computational power, the use of numerical modelling and simulation in industry and academia has increased the past decades. These numerical models and simulations can be used to study phenomena that would otherwise be expensive, difficult or even impossible to study otherwise, such as rock drilling in geothermal applications. The purpose of this chapter is to present the numerical model that has been developed within this thesis. The first section covers the conventional Bonded-Particle Method (BPM) for the Discrete Element Method (DEM). The BPM for DEM forms the foundation of the newly developed statistical model for heterogeneous brittle materials, presented in the second section of this chapter.

4.1 The Bonded Discrete Element Method

A widely popular numerical tool for modelling the mechanical behaviour of granular assemblies is the Discrete Element Method (DEM). In the original formulation by Cundall and Strack [44], the granular material is modelled using several discrete, rigid spheres. A key feature about the DEM is the individual treatment of each element - the motion of each sphere is resolved through the integration of Newtons second law,

$$m_i \frac{d\boldsymbol{v}_i}{dt} = \boldsymbol{F}_i \tag{4.1}$$

where m_i and $\boldsymbol{v}_i$ are the mass and velocity of particle i, respectively. The total force acting on particle i may be expressed as

$$\boldsymbol{F}_i = \boldsymbol{F}_i^{ext} + \boldsymbol{F}_i^{damp} + \sum_{j=1}^{n_j} \boldsymbol{F}_{ij} \tag{4.2}$$

where $\boldsymbol{F}_i^{ext}$ is the external forces, $\boldsymbol{F}_i^{damp}$ is the damping forces and $\boldsymbol{F}_{ij}$ is the contact forces between particles i and j. Typically, the integration of Eq.(4.1) is done explicitly, from which the acceleration, velocity and position is obtained for each time step. The angular motion is governed by

$$\boldsymbol{I}_i \frac{d\boldsymbol{\omega}_i}{dt} = \sum_j \boldsymbol{M}_{ij} \tag{4.3}$$

where $\boldsymbol{I}_i$ and $\boldsymbol{\omega}_i$ is the moment of inertia and angular velocity of particle i respectively and $\boldsymbol{M}_{ij}$ is the applied torque from particle j. In the present work, the contact forces are represented by a linear spring-dashpot model for both the normal and shear direction [65, 66]. In total, there are five governing DEM parameters that are relevant for the particle-particle interactions in this study: normal and shear spring constants, k_n and k_s, normal and tangential damping coefficients, c_n and c_t, as well as sliding friction μ.

An important milestone in the development of the DEM is the Bonded Particle Model (BPM) for rock, formulated by Potyondy and Cundall [43]. Here, the rock is approximated as an assembly of cemented particles. This cementing, or bonding, of the particles works in parallel with the standard DEM formulation. These bonds exists at contact points and breaks instantaneously and permanently once the stress state in the bond reaches a prescribed maximum value. The failure criteria is expressed as

$$\bar{\sigma}^{\max} = \frac{-\bar{F}^{\mathrm{n}}}{A} + \frac{\left|\bar{M}^{\mathrm{s}}\right| \bar{R}}{I} \geq \sigma_c \tag{4.4}$$

$$\bar{\tau}^{\max} = \frac{\left|\bar{F}^{\mathrm{s}}\right|}{A} + \frac{\left|\bar{M}^{\mathrm{n}}\right| \bar{R}}{J} \geq \tau_c \tag{4.5}$$

where I and J are the moment and polar moment of inertia of the bond and A is the bond area. The radius of the bond between two particles A and B is given as the minimum of the bonding particles radii, i.e. $\bar{R} = \bar{\lambda}\, min(R^A, R^B)$, where $\bar{\lambda}$ is the radius multiplier. The tensile and shear bond strengths are represented by σ_c and τ_c, respectively, and the bond breaks permanently and instantaneously once either the tensile stress or shear stress exceeds its limit value. The bond forces ($\bar{F}^n$ and $\bar{F}^s$) and moments ($\bar{M}^n$ and $\bar{M}^s$) are calculated incrementally each time step according to

$$\begin{cases} \Delta \bar{F}^n = \bar{k}^n A \Delta U^n \\ \Delta \bar{F}^s = -\bar{k}^s A \Delta U^s \\ \Delta \bar{M}^{\mathrm{n}} = -\bar{k}^s J \Delta \theta^n \\ \Delta \bar{M}^s = -\bar{k}^n I \Delta \theta^s \end{cases} \tag{4.6}$$

where $\bar{k}^n$ and $\bar{k}^s$ are the normal and shear bond stiffnesses, respectively, and the relative displacement and rotation in the normal and shear direction are represented by $\Delta U^{n/s}$ and $\Delta \theta^{n/s}$. The damage in the rock is represented directly via the breakage of the bonds. This means that the initiation, propagation and coalescence of cracks are naturally described using this model. The crack initiates on a microscopic scale with a broken bond, propagates through the media through more broken bonds and coalesce with other cracks to form larger fracture planes. The BPM also utilize a local non-viscous damping $\bar{\alpha}$ in order to account for the energy dissipation from e.g. internal friction. Lastly, the amount of particle interlocking is controlled via the interlocking range $\bar{\beta}$.

Apart from the particle radius, the BPM-DEM approach consists of 11 input parameters, whereof five of them are related to the DEM, k_n, k_s ,c_n, c_s and μ, and six of them are related to the bonds between the particles, $\bar{k}_n$, $\bar{k}_s$, $\bar{\sigma}_c$, $\bar{\tau}_c$, $\bar{\beta}$ and $\bar{\alpha}$. A drawback with the BPM-DEM is the extensive calibration procedure required to obtain these parameters, and this is a topic that has been explored by previous authors. For example, the local constitutive model by Oñate et al. [67] or the calibration scheme by Wang and Tonon [68].

4.2 A new approach for modelling rock

The numerical model for brittle heterogeneous materials presented in this section introduces the heterogeneity in the conventional BPM-DEM approach in two ways. Firstly, a grain shape heterogeneity is introduced as random, irregular ellipsoids. Secondly, the intragranular structure is constructed using parallel bonds with microscopic parameters that are given by the Weibull distribution [41]. Four micromechanical parameters, the normal and shear stiffness and the tensile and shear strength, are governed by the distribution and the probability density function for a micromechanical parameter η is given by [41]

$$f(\eta, \eta_0, m) = \frac{m}{\eta_0} \Big(\frac{\eta}{\eta_0} \Big)^{m-1} e^{-(\eta/\eta_0)^m} \tag{4.7}$$

where η_0 is the scale parameter and m is the shape parameter (or heterogeneity index). A larger parameter spread is obtained for a lower value of the shape parameter m, which means that a smaller value of the shape parameter corresponds

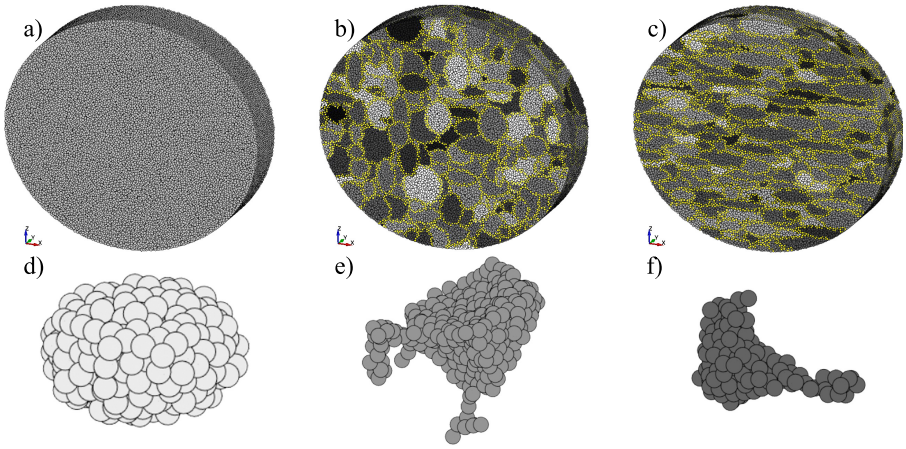

Figure 4.1: The grain generation process of samples for the BDT. The different gray scale colouring represents the mean micromechanical strength of the grains. Initial node distribution a), an example of a sample with equal grain radii distributions for x, y and z b), an example of an anisotropic sample with a preferred grain direction, i.e. the radii distribution in the x-direction is larger than for the other directions c), example of a regular ellipsoid shape d) and examples of irregular grain shapes e-f).

to a more heterogeneous distribution of the microparameter. For the case of a significantly large value of the shape parameter, such as 10^6, the distribution is practically constant. For a given sample geometry discretized with rigid spheres of uniform size, such as the one in Figure 4.1 a), the grains were distributed throughout the body by performing the following steps:

1. A parent node is randomly selected within the domain and the mean grain micromechanical properties are obtained from the Weibull distribution.

2. A randomized ellipsoid is created around the parent node by generating the radii uniformly, i.e.

$$R_x, R_y, R_z \sim U(R_{min}, R_{max}) \tag{4.8}$$

   where $U(R_{min}, R_{max})$ is the uniform distribution between R_{min} and R_{max}.

3. All particles within the ellipsoid are bound together within ± 10 % of the mean grain values and then excluded from future grain bonding.

4. Steps 1)-3) are repeated until no particles were left.

An example of a generated sample for the BDT can be seen in Figure 4.1 b), where $R_x = R_y = R_z$. An example of grains with a preferred direction can be seen in the BDT in Figure 4.1 c), where the grains are slightly elongated in the x-direction. The first few grains that are generated are likely to be ellipsoidal, as seen in Figure 4.1 d). As more particles are excluded from bonding, more irregular grain shapes are obtained, such as the ones seen in Figure 4.1 e-f). For the generated samples in Figure 4.1, the grey scale colouring denotes the average strengths of the grains, with black denoting the weakest grains.

Grain cementing model

In order to obtain a statistical variation in the interganular binding, a cementing model with properties based on the grains being bound is used. Here, the parallel bond properties of the cement between two grains depend on one of the grains being cemented. Given a rock body with distributed grains, the cementing process is as follows. A grain G_i is selected and its neighbouring grains G_j are identified as the grains that are within the interlocking range. In other words, G_j is a neighbour of G_i if, for all sets of distances d_{ij} between constituent particles of the two grains, any $d_{ij} \leq \bar{\beta}$. The particles of G_j within interlocking range of G_i are then cemented together using parallel bonds with normal and shear strengths according to

$$\begin{cases} \bar{\sigma}_c^{ij} = C_f \cdot \bar{\sigma}_c^i \\ \bar{\tau}_c^{ij} = C_f \cdot \bar{\tau}_c^i \end{cases} \tag{4.9}$$

where $\bar{\sigma}_c^{ij}$ and $\bar{\tau}_c^{ij}$ are the normal and shear bond strength of the cement, respectively. $\bar{\sigma}_c^i$ and $\bar{\tau}_c^i$ are the mean normal and shear bond strengths of grain G_i, respectively, and C_f is the cement scaling parameter. The grain boundaries are denoted by yellow particles, e.g. as in Figure 4.1, however, only half of the boundary nodes are shown due to clarity.

Chapter 5

Summary of appended papers

In this chapter, the methodology and results of the appended papers are briefly summarized.

5.1 Paper A: A Statistical DEM Approach for Modelling Heterogeneous Brittle Materials

Brittle and heterogeneous materials like rocks usually exhibit a large spread in the experimental data and there is a need for a stochastic model that can mimic this behaviour. In Paper A, a new numerical approach, based on the Bonded Discrete Element Method, for modelling of heterogeneous brittle materials is proposed and evaluated. The material properties are introduced into the model via two main inputs. Firstly, a grain shape heterogeneity is introduced as random, irregular ellipsoids. Secondly, the micromechanical parameters of the constituent particles of the grains are given by the Weibull distribution. The model was applied on the Brazilian Disc Test, where the crack initiation, propagation, coalescence and branching could be investigated for different sets of grain cement strengths and sample heterogeneities. The damages prior and after failure for three different cement strengths are shown in From Figures 5.1. It is clear that for a higher cement strength, the crushed zone close to the loading jaws is more prevalent compared to the weaker cement strengths. This explains the higher amount of cracks initiated close to loading jaws for cases with higher cement strength. It can also be seen from Figure 5.1 that a more severe zigzag pattern was observed for lower cement strengths, which can be explained by the fact that cracks propagate in a direction of least resistance. Generally, the proposed model was found to capture well typical phenomena associated with the fracture process of brittle

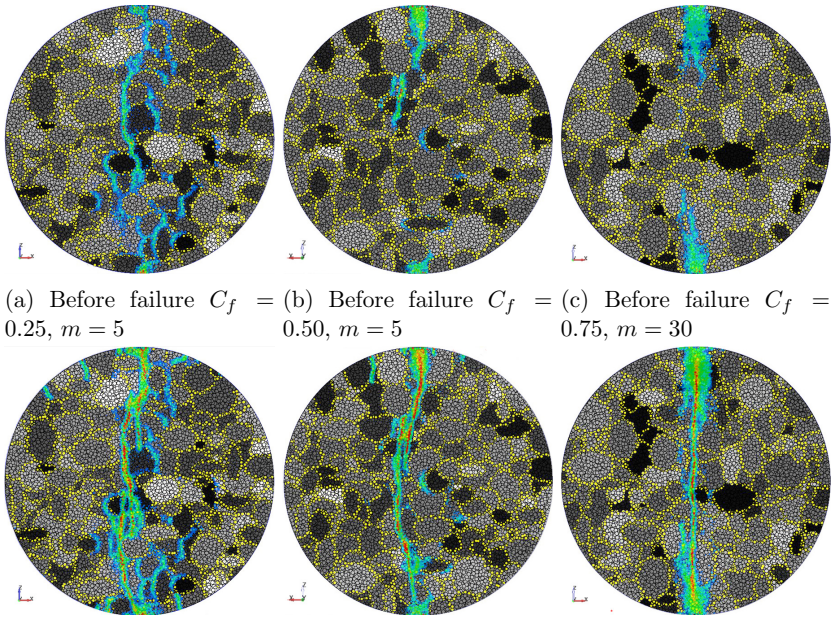

(a) Before failure $C_f = 0.25$, $m = 5$ (b) Before failure $C_f = 0.50$, $m = 5$ (c) Before failure $C_f = 0.75$, $m = 30$

(d) After failure $C_f = 0.25$, $m = 5$ (e) After failure $C_f = 0.50$, $m = 5$ (f) After failure $C_f = 0.75$, $m = 30$

Figure 5.1: Examples of accumulated damage right before failure for cement strength 0.25 a), 0.50 b) and 0.75 c), and the corresponding final crack paths d-f). Particle colour represents the loss of bonds, i.e. a red particle has loss all of its bonds while the bonds of a blue particle remains intact.

heterogeneous materials, e.g. the the unpredictability of the strength in tension and crack properties.

5.2 Paper B: Static and Dynamic Properties of Kuru Black Diorite and Grey Granite Using Full-Field Deformation Measurements

In Paper B, the static and dynamic properties of two rock materials - Kuru grey granite and Kuru black diorite were obtained. The rock materials were subjected to compressive and indirect tensile loading by uniaxial compression (UCT) and Brazilian disc tests (BDT), respectively. To obtain the dynamic properties, a

Split-Hopkinson Pressure Bar device was utilized. In order to capture onset of unstable crack growth with high precision, and the subsequent propagation, images were captured with a high-speed camera at a frame rate of 663,000 fps. The exterior deformation fields of the samples were evaluated by using digital image correlation (DIC). An example of an evaluated dynamic UCT of Kuru black diorite is shown in Figure 5.2. The dynamic compressive stress vs axial strain response and the corresponding strain rate vs axial strain history are shown as black and blue curves, respectively. The strain rate becomes nearly constant, approx. 300 s^{-1}, at stress levels corresponding to the linear elastic stage and the stage of stable crack growth. The read star marks the instant when the first visible crack was detected (Figure 5.2c). This instant corresponds to the onset of unstable crack growth and the compressive crack-damage stress was, for this specific test, approx. 83 % of the peak strength. In the two following images, Figure 5.2d and e, the complete failure is shown. In Figure 5.3, an example of a dynamic BDT of Kuru grey granite is presented. In Figure 5.3a-c, the indirect tensile strain fields are shown. In the subsequent image, a crack can clearly be observed (Figure 5.3d) at the location of prior localized tensile strain. It is clear from Figure 5.3 that the crack initiates well before the peak stress. The tensile crack-damage stress was approx. 80 % of the peak stress value. By evaluating the deformation fields with DIC a strain rate of approx. 150 s^{-1} was reached. Hence, using the peak strengths as the characteristic strengths risking overestimation of the load bearing capacity. The presented experiments show how the crack-damage stresses can be determined in compression as well as tension. These values will be used as input in coming numerical studies of percussive rock drilling. All experimental results are presented in Paper B.

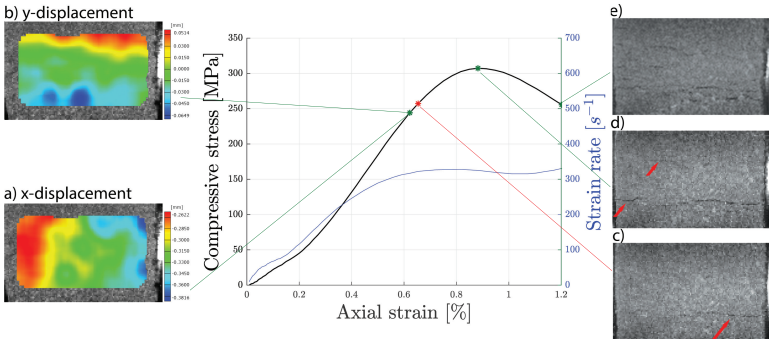

Figure 5.2: Dynamic compressive stress versus axial for KBD. The displacement fields in the loading direction and transverse direction just below the crack damage stress a-b), the frame at which the first crack is visible c), post-peak cracks d-e).

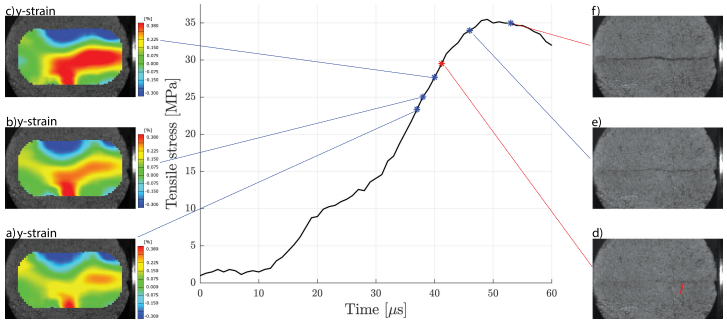

Figure 5.3: High-speed image and DIC at certain stages of a dynamic BDT of Kuru Black diorite (KBD). The strain field across the loading direction at three different stages before crack initiation a-c), first visible crack d) and crack propagation e-f).

Chapter 6

Discussion, conclusions and outlook

This thesis has focused on the numerical and experimental evaluation of the rock fracture process. For the numerical part, a new approach for modelling brittle heterogeneous materials was proposed and used to evaluate the Brazilian disc test. The heterogeneity was introduced as irregular grain shapes with micromechanical parameters governed by the Weibull distribution. By generating and simulating a large set of samples, the effects that the parameters, grain cement strength and heterogeneity, had on the initiation, propagation and coalescence of cracks were evaluated. Furthermore the effect the parameters had on the on the tensile strength was derived. In the experimental work, the static and dynamic properties of Kuru grey granite and Kuru black diorite were obtained by uniaxial compression and Brazilian disc tests. For the dynamic testing, a Split-Hopkinson Pressure Bar was used, and a high-speed camera captured the initiation and propagation of cracks during the tests. The exterior deformation fields were obtained from Digital Image Correlation (DIC).

The proposed numerical model based on BPM-DEM was able to reproduce unpredictable behaviours typically observed for these types of materials. For example variations in predicted tensile strength, initiation, propagation and coalescence of cracks and anisotropic behaviour for materials with grains having preferred orientation. The numerical study also gave insights about the Brazilian disc test itself, e.g. that the test seems to perform worse for materials that can be considered to have a high grain cement strength. Also, the numerical model was applied on a rather small scale in this study, but the methodology should work for large scale problems as well, e.g. for modelling varying ground materials in rock drilling.

The high-speed photography of the Dynamic UCT gave insight about the fracture process of rock. The inertia associated with crack tip opening limits the

propagation, and as the load is rapidly increasing, new cracks are initiated before previous cracks grow unstable. Kuru black diorite was also found to be more sensitive to the deformation rate compared to the Kuru grey granite. It was also found that the crack-damage stress in the dynamic UCT were approx. 90 % of the peak stress, which is slightly more than the quasi-static value. For the dynamic BDT, the main splitting crack could be seen to initiate at 65 and 79 % of the peak stress for the diorite and granite, respectively. This suggests that the peak value of the transmitted stress wave significantly overestimates the dynamic tensile strength, i.e. the load bearing capacity, and that high-speed photography should be used to monitor the test.

In the near future, the numerical model based on BPM-DEM will be calibrated by using the obtained static and dynamic properties of the investigated rocks. Furthermore, other parameters such as sizes and shapes of the grains will be studied. The model will also be further developed to incorporate strain rate dependency in the breakage of the bonds.

References

[1] O. Kuhn. *Ancient Chinese drilling*. 2004.

[2] G. West. *Innovation and the Rise of the Tunneling Industry*. 1st ed. New York: Cambridge University Press, 1988.

[3] D. Zou. *Theory and technology of rock excavation for civil engineering*. 2016, pp. 1–699.

[4] C. Bu, Y. Qu, Z. Cheng, and B. Liu. Numerical simulation of impact on pneumatic DTH hammer percussive drilling. *Journal of Earth Science* 20.5 (2009), pp. 868–878.

[5] M. Saadati. "On the mechanical behavior of granite : Constitutive modeling and application to percussive drilling". PhD thesis. 2015.

[6] T. Saksala, M. Fourmeau, P.A. Kane, and M. Hokka. 3D finite elements modelling of percussive rock drilling: Estimation of rate of penetration based on multiple impact simulations with a commercial drill bit. *Computers and Geotechnics* 99.February (2018), pp. 55–63.

[7] H. Shariati. *Mechanical modeling of granite subjected to contact loading*. 2019.

[8] Y. Melamed, A. Kiselev, and M. Gelfgat. "Hydraulic Hammer Drilling Technology: Developments and Capabilities". *Annual International Energy Week Conference*. Vol. 8. 1997.

[9] R.J. Plinninger. Abrasiveness Assessment for Hard Rock Drilling. *Geomechanik und Tunnelbau* 1.1 (2008), pp. 38–46.

[10] M. Hokka, J. Black, D. Tkalich, M. Fourmeau, A. Kane, H. Hoang, C.C. Li, W.W. Chen, V.-T.T. Kuokkala, N.H. Hoang, C.C. Li, W.W. Chen, and V.-T.T. Kuokkala. Effects of strain rate and confining pressure on the compressive behavior of Kuru granite. *International Journal of Impact Engineering* 91.February (2016), pp. 183–193.

[11] P.A. Hsieh. *Fundamentals of Rock Mechanics*. Vol. 9. 3. 2009.

[12] J.F. Labuz and J.M. Bridell. Reducing frictional constraint in compression testing through lubrication. *International Journal of Rock Mechanics and Mining Sciences and* 30.4 (1993), pp. 451–455.

[13] A. Basu, D.A. Mishra, and K. Roychowdhury. Rock failure modes under uniaxial compression, Brazilian, and point load tests. *Bulletin of Engineering Geology and the Environment* 72.3-4 (2013), pp. 457–475.

[14] S. Chakraborty, R. Bisai, S.K. Palaniappan, and S.K. Pal. Failure modes of rocks under uniaxial compression tests: an experimental approach. *Journal of Advances in Geotechnical Engineering* 2.3 (2019), pp. 1–8.

[15] F. Carneiro. "A new method to determine the tensile strength of concrete." *5th meeting of the Brazilian Association for Technical Rules*. 1943.

[16] T. Akazawa. New test method for evaluating internal stress due to compression of concrete: the splitting tension test. *Japan Society of Civil Engineers* 29 (1943), pp. 777–787.

[17] D. Li and L.N.Y. Wong. The brazilian disc test for rock mechanics applications: Review and new insights. *Rock Mechanics and Rock Engineering* 46.2 (2013), pp. 269–287.

[18] C. Fairhurst. "Laboratory Measurements of Some Physical Properties of Rock". *The 4th U.S. Symposium on Rock Mechanics (USRMS)*. 1961.

[19] P. Colback. An analysis of brittle fracture initiation. *1st ISRM Congress* (1966), pp. 385–391.

[20] M. Mellor and I. Hawkes. Measurement of tensile strength by diametral compression of discs and annuli. *Engineering Geology* 5.3 (1971), pp. 173–225.

[21] R. Yuan and B. Shen. Numerical modelling of the contact condition of a Brazilian disk test and its influence on the tensile strength of rock. *International Journal of Rock Mechanics and Mining Sciences* 93.December 2015 (2017), pp. 54–65.

[22] Y. Jianhong, F.Q. Wu, and J.Z. Sun. Estimation of the tensile elastic modulus using Brazilian disc by applying diametrically opposed concentrated loads. *International Journal of Rock Mechanics and Mining Sciences* 46.3 (2009), pp. 568–576.

[23] S. Patel and C.D. Martin. Application of Flattened Brazilian Test to Investigate Rocks Under Confined Extension. *Rock Mechanics and Rock Engineering* 51.12 (2018), pp. 3719–3736.

[24] L. Yawei and G. Ahmad. Rock failure behavior and brittleness under the confined Brazilian test. *52nd U.S. Rock Mechanics/Geomechanics Symposium* 2 (2018).

[25] G. Subhash. Split-Hopkinson Pressure Bar Testing of Ceramics Review of Traditional Split-Hopkinson Pressure Bar Operational Principles. 8 (2000), pp. 497–504.

[26] H. Kolsky. An investigation of the mechanical properties of materials at very high rates of loading. *Proceedings of the Physical Society. Section B* 62.11 (1949), pp. 676–700.

[27] K. Xia, M.H. Nasseri, B. Mohanty, F. Lu, R. Chen, and S.N. Luo. Effects of microstructures on dynamic compression of Barre granite. *International Journal of Rock Mechanics and Mining Sciences* 45.6 (Sept. 2008), pp. 879–887.

[28] D.J. Frew, S.A. Akers, W. Chen, and M.L. Green. Development of a dynamic triaxial Kolsky bar. *Measurement Science and Technology* 21.10 (2010).

[29] T. Saksala, M. Hokka, V.T. Kuokkala, and J. Mäkinen. Numerical modeling and experimentation of dynamic Brazilian disc test on Kuru granite. *International Journal of Rock Mechanics and Mining Sciences* 59 (2013), pp. 128–138.

[30] Q.B. Zhang and J. Zhao. A review of dynamic experimental techniques and mechanical behaviour of rock materials. *Rock Mechanics and Rock Engineering* 47.4 (2014), pp. 1411–1478.

[31] R.D. Perkins and S.J. Green. High speed photography in dynamic materials testing. *Review of Scientific Instruments* 39.8 (1968), pp. 1209–1210.

[32] M. Cai, P.K. Kaiser, F. Suorineni, and K. Su. A study on the dynamic behavior of the Meuse/Haute-Marne argillite. *Physics and Chemistry of the Earth* 32.8-14 (Jan. 2007), pp. 907–916.

[33] D. Ai, Y. Zhao, Q. Wang, and C. Li. Experimental and numerical investigation of crack propagation and dynamic properties of rock in SHPB indirect tension test. *International Journal of Impact Engineering* 126.January (2019), pp. 135–146.

[34] D. Ai, Y. Zhao, B. Xie, and C. Li. Experimental study of fracture characterizations of rocks under dynamic tension test with image processing. *Shock and Vibration* 2019 (2019).

[35] P. Pei, F. Dai, Y. Liu, and M. Wei. Dynamic tensile behavior of rocks under static pre-tension using the flattened Brazilian disc method. *International Journal of Rock Mechanics and Mining Sciences* 126.December 2019 (2020), p. 104208.

[36] J. Kajberg and M. Sjödahl. Optical Method to Study Material Behaviour at High Strain Rates. *IUTAM Symposium on Field Analyses for Determination of Material Parameters - Experimental and Numerical Aspects* (2003), pp. 37–49.

[37] J. Kajberg and B. Wikman. Viscoplastic parameter estimation by high strain-rate experiments and inverse modelling - Speckle measurements and high-speed photography. *International Journal of Solids and Structures* 44.1 (2007), pp. 145–164.

[38] M. Ju, J. Li, Q. Yao, X. Li, and J. Zhao. Rate effect on crack propagation measurement results with crack propagation gauge, digital image correlation, and visual methods. *Engineering Fracture Mechanics* 219.March (2019), p. 106537.

[39] Q.B. Zhang and J. Zhao. Determination of mechanical properties and full-field strain measurements of rock material under dynamic loads. *International Journal of Rock Mechanics and Mining Sciences* 60 (2013), pp. 423–439.

[40] M. Saadati, P. Forquin, K. Weddfelt, P.L. Larsson, and F. Hild. Granite rock fragmentation at percussive drilling - experimental and numerical investigation. *International Journal for Numerical and Analytical Methods in Geomechanics* 38.8 (2014), pp. 828–843.

[41] W. Weibull. Wide applicability. *Journal of applied mechanics* 103 (1951), pp. 293–297.

[42] M. Saadati, P. Forquin, K. Weddfelt, and P.L. Larsson. On the tensile strength of granite at high strain rates considering the influence from preexisting cracks. *Advances in Materials Science and Engineering* 2016 (2016).

[43] D.O. Potyondy and P.A. Cundall. A bonded-particle model for rock. *International Journal of Rock Mechanics and Mining Sciences* 41.8 SPEC.ISS. (2004), pp. 1329–1364.

[44] P.A. Cundall and O.D.L. Strack. A discrete numerical model for granular assemblies. *Géotechnique* 29.1 (Mar. 1979), pp. 47–65.

[45] H. Huang, E. Detournay, B. Lecampion, and E. Detournay. Discrete element modeling of tool-rock interaction II: Rock indentation. *International Journal for Numerical and Analytical Methods in Geomechanics* 37 (2013), pp. 1913–1929.

[46] X. Zhu, W. Liu, and X. He. The investigation of rock indentation simulation based on discrete element method. *KSCE Journal of Civil Engineering* 21.4 (2017), pp. 1201–1212.

[47] H. Huang, B. Lecampion, and E. Detournay. Discrete element modeling of tool-rock interaction I: Rock cutting. *International Journal for Numerical and Analytical Methods in Geomechanics* 37 (2013), pp. 1913–1929.

[48] J. Rojek. Discrete element thermomechanical modelling of rock cutting with valuation of tool wear. *Computational Particle Mechanics* 1.1 (2014), pp. 71–84.

[49] N. Cho, C.D. Martin, and D.C. Sego. A clumped particle model for rock. *International Journal of Rock Mechanics and Mining Sciences* 44.7 (2007), pp. 997–1010.

[50] L. Scholtès, F.V. Donzé, F. Donze, and F.V. Donzé. A DEM model for soft and hard rocks: Role of grain interlocking on strength. *Journal of the Mechanics and Physics of Solids* 61.2 (2013), pp. 352–369.

[51] T. Ma, N. Peng, Z. Zhu, Q. Zhang, C. Yang, and J. Zhao. Brazilian tensile strength of anisotropic rocks: Review and new insights. *Energies* 11.2 (2018).

[52] D.M. Ivars, D.O. Potyondy, and I.C. Group. "The Smooth-Joint Contact Model". *8th. World Congress on Computational Mechanics (WCCM8)*. July. 2015, pp. 29–31.

[53] D.O. Potyondy. A grain-based model for rock: Approaching the true microstructure. *Bergmekanikk i Norden 2010 - Rock Mechanics in the Nordic Countries* June 9-12, 2010 (2010), pp. 225–234.

[54] U. Beste. On the Nature of Cemented Carbide Wear in Rock Drilling. *Science And Technology* (2004), p. 78.

[55] D.R. Prothero and F. Schwab. *Sedimentary Geology*. Vol. 206. 4419. 1979, pp. 677–677.

[56] W. Petruk. *Applied mineralogy*. 2000, pp. 135–147.

[57] R. DiPippo. *Geothermal Power Generation: Developments and Innovation*. 2016, pp. 1–822.

[58] W.F. Brace, B.W. Paulding, and C. Scholz. Dilatancy in the fracture of crystalline rocks. *Journal of Geophysical Research* 71.16 (1966), pp. 3939–3953.

[59] ISRM. Suggested Methods for Determining the Uniaxial Compressive Strength and Deformability of Rock Materials. *International Society for Rock Mechanics* December (1977), pp. 0–3.

[60] Hondros. The evaluation of Poisson's ratio and the modulus of materials of low tensile resistance by the Brazilian (indirect tensile) test with particular reference to concrete. *Aust. J. Appl. Sci.* 10 (1959), pp. 243–268.

[61] ISRM. Suggested Methods for Determining Tensile Strength of Rock Materials - 1. Suggested Method for Determining Direct Tensile Strength. *International Journal of Rock Mechanics and Mining Sciences* 15.3 (1978), pp. 99–103.

[62] C. Fairhurst. On the validity of the 'Brazilian' test for brittle materials. *International Journal of Rock Mechanics and Mining Sciences and* 1.4 (1964), pp. 535–546.

[63] J.J. Swab, J. Yu, R. Gamble, and S. Kilczewski. Analysis of the diametral compression method for determining the tensile strength of transparent magnesium aluminate spinel. *International Journal of Fracture* 172.2 (2011), pp. 187–192.

[64] G.T. Gray. Classic Split-Hopkinson Pressure Bar Testing, in: ASM Metals Handbook: Mechanical Testing and Evaluation, vol. 8, ASM International, Metals Park (OH). 8 (2000), pp. 462–476.

[65] N. Karajan, Z. Han, H. Teng, and J. Wang. On the Parameter Estimation for the Discrete-Element Method in LS-DYNA ®. *13 th International LS-DYNA Users Conference* (2014), pp. 1–9.

[66] LSTC. Keyword User ' S Manual Volume 1. *Livermore Software Technology Corporation (LSTC)* I.12 (2020), p. 2350.

[67] E. Oñate, F. Zárate, J. Miquel, M. Santasusana, M.A. Celigueta, F. Arrufat, R. Gandikota, K. Valiullin, L. Ring, F. Zarate, J. Miquel, M. Santasusana Isach, M.A. Celigueta, F. Arrufat, R. Gandikota, K. Valiullin, and L. Ring. A local constitutive model for the discrete element method. Application to geomaterials and concrete. *Computational Particle Mechanics* 2.2 (2015), pp. 139–160.

[68] Y. Wang and F. Tonon. Modeling Lac du Bonnet granite using a discrete element model. *International Journal of Rock Mechanics and Mining Sciences* 46.7 (2009), pp. 1124–1135.

Department of Engineering Sciences and Mathematics
Division of Solid Mechanics

ISSN 1402-1757
ISBN 978-91-7790-836-4 (print)
ISBN 978-91-7790-837-1 (pdf)

Tryck: Lenanders Grafiska, 136467

LULEÅ
UNIVERSITY
OF TECHNOLOGY